Ground State Phase Transitions in the 2-Site XY Model

Ziyue Zhang

Advised by Prof. James Freericks

Georgetown University

Department of Physics

May 2021

Abstract

Adiabatic state preparation, which involves starting a quantum system in an easy-to-prepare ground state and slowly changing the Hamiltonian to a complex one while keeping the system in the ground state, is a powerful tool for preparing ground states of systems with complex Hamiltonians. By combining this method with the computational advantages of quantum computers, adiabatic state preparation has the potential to solve important quantum mechanical problems that cannot be solved with classical computing. However, for systems with ground states determined by different quantum numbers conserved by symmetries of the Hamiltonian, adiabatic state preparation fails. This thesis demonstrates a generalization of adiabatic state preparation that overcomes this challenge by explicitly breaking the symmetry of the Hamiltonian. Here, the ground-state phase diagram of the one-dimensional two-site XY model, a ferromagnetic model for spin-$\frac{1}{2}$ particles, is calculated using this generalized procedure. The experimental results from quantum hardware are comparable with the exact solutions of the system. As quantum computing hardware becomes more robust, this procedure can be used to solve even larger systems and prepare even more ground-state phase diagrams.

Acknowledgements

Thank you so much to Ephrata Zelleke for laying the foundation for my thesis. Her advice was crucial for my success at the beginning of the project.

I would also like to thank Akhil Francis who was there to answer all of my questions, no matter how simple, during the most crucial occasions. Akhil's thoughtfulness and excitement was incredible. He would always have the upmost patience, and I am incredibly grateful for his guidance.

A tremendous and heartfelt thank you to Professor Freericks for his care and attention. I am incredibly grateful for the countless hours that he spent with me virtually. Professor Freericks injected me with confidence and taught me an incredible depth of information. I am so blessed that he shared with me his experience and expertise.

Finally, in an unusual and difficult year, thank you to my friends and family for supporting me. Through many hardships, you were there remind me of my values. For that, I am eternally grateful.

Contents

Chapter 1

Introduction

1.1 Preview and Units

Modern development in quantum computing has been accompanied with a flurry of research in algorithms and techniques designed to take advantage of its superior computing capabilities. Adiabatic state preparation is one such technique that is designed to prepare the ground state of systems with complex Hamiltonians by initializing an easy-to-prepare ground state and evolving the system slowly. The ability to prepare a robust ground state through adiabatic state preparation would have important consequences in quantum computing. However, as will be shown in this thesis, adiabatic state preparation cannot be used to prepare the ground state of the one-dimensional XY model and other systems whose Hamiltonian commutes with their measurement operator. This thesis will use a procedure that overcomes this challenge by explicitly breaking the symmetry of the XY Hamiltonian through the addition of a magnetic field in the x-direction. It will be shown that the phase transitions of the one-dimensional 2-site XY model can be calculated in a quantum computer using adiabatic state preparation after breaking the symmetry of the system. Our final results are comparable to the known exact phase transitions of the model.

The Ising and XY models will be introduced in this thesis. Both models describe interactions between spin-$\frac{1}{2}$ particles and use an explicit Pauli matrix representation. To simplify calculations that require spin measurements, the remainder of the thesis will use dimensionless units where $\hbar = 1$ and the quantum mechanical spins of spin-$\frac{1}{2}$ particles,

$\frac{\hbar}{2}$ and $-\frac{\hbar}{2}$, are rescaled and represented as 1 and -1, respectively. An eigenstate with a z-component of spin of 1 will correspond with the eigenspinor $|\uparrow\rangle$, and an eigenstate with a z-component of spin of -1 will correspond with the eigenspinor $|\downarrow\rangle$. Furthermore, the magnitude of magnetic fields introduced in this paper will be expressed as the dimensionless magnetic moment proportional to the Bohr magneton, μ_B.

1.2 The Ising Model

Many quantum mechanical and statistical models exist to describe ferromagnetism arising from spin-$\frac{1}{2}$ particles arranged in different dimensional lattices. The one-dimensional Ising model is the simplest model in this group and will be characterized to provide a preview for the one-dimensional XY Model.

The one-dimensional Ising model describes spins on a one-dimensional lattice with interactions between neighboring lattice sites [1]. By convention, each lattice site has a z-component of spin degree of freedom. For a system of N lattice sites, the model is expressed as

$$\mathbf{H}_{Ising} = -\sum_{\langle i\, j\rangle}^{N} J_{ij}\sigma_i^z\sigma_j^z \ , \tag{1.1}$$

where J_{ij} is the spin exchange coefficient that describes the interaction between spins at neighboring sites i and j, $\langle i\ j\rangle$ denotes nearest neighbor lattice sites, and the Pauli matrix σ_k^z is used to calculate the z-component of spin at lattice site k. In the ground state, spins line up in the same direction. A magnetic field, B, that is longitudinal to the spins can also be introduced into the system and modifies the Hamiltonian to

$$\mathbf{H}_{Ising} = -\sum_{\langle i\, j\rangle}^{N} J_{ij}\sigma_i^z\sigma_j^z - B\sum_{i=1}^{N}\sigma_i^z \ . \tag{1.2}$$

Because the Hamiltonian in Eq. (1.2) commutes with $\mathbf{S}^z$, the operator for the z-component of spin, measuring the total z-component of spin, m_z, is a good quantum number to describe

the eigenstate of the system. $\mathbf{S}^z$ is defined as $\mathbf{S}^z = \sum_i \sigma_i^z$ ($\mathbf{S}^z = \sum_i \frac{\hbar}{2}\sigma_i^z$ in conventional units). Depending on the quantum number of a given eigenstate, varying the magnitude of B would not change its energy if $\sum_{i=1}^{N} B_z\sigma_i^z = 0$ and would change its energy otherwise. As B varies, if the energy of an eigenstate with a given quantum number varies faster than that of another eigenstate with a different quantum number, then the energies of the two eigenstates will eventually intersect at some B. This point is called a level crossing. If a system remains in its ground state or excited state, the system will undergo a phase transition, or change quantum numbers, at a level crossing.

Consider a 2-site one-dimensional Ising model with $J_{12} = J_{21} > 0$ in a longitudinal field $B = B_1 = B_2 > 0$. The 2-site model has four product states, or four possible tensored eigenstates arising from the possible combinations of the z-component of spin at each of the two lattice sites. The product states of the system are eigenstates of the Hamiltonian with energies

$$H\left|\uparrow\uparrow\right\rangle = (-2J_{12} - 2B)\left|\uparrow\uparrow\right\rangle \tag{1.3}$$

$$H\left|\uparrow\downarrow\right\rangle = 2J_{12}\left|\uparrow\downarrow\right\rangle \tag{1.4}$$

$$H\left|\downarrow\uparrow\right\rangle = 2J_{12}\left|\downarrow\uparrow\right\rangle \tag{1.5}$$

$$H\left|\downarrow\downarrow\right\rangle = (-2J_{12} + 2B)\left|\downarrow\downarrow\right\rangle \ . \tag{1.6}$$

A plot of the energies in Eqs. (1.3)-(1.6) in Figure 1.1 reveals that the magnetic field induces a level crossing between the $m_z = -1$ and $m_z = 1$ eigenstates and the $m_z = 0$ and $m_z = -1$ eigenstates. For a system required to stay in the excited state, the system would transition from a quantum number of $m_z = -1$ to a quantum number of $m_z = 0$ as B increases.

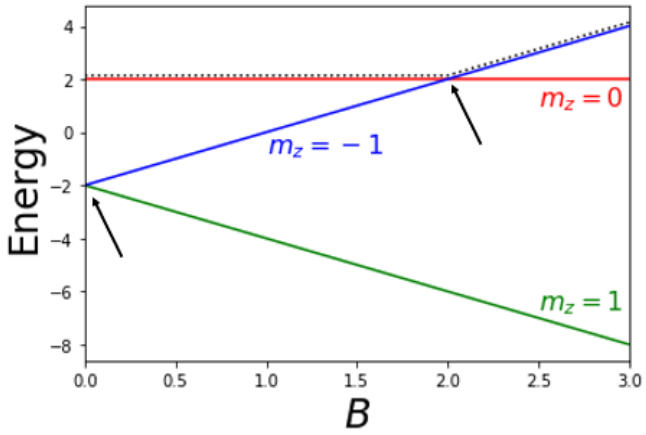

Figure 1.1: Energies of a 2-site Ising model over a varying magnetic field, B. The figure assumes a constant $J_{12} = J_{21} = 1$ and $J_{11} = J_{22} = 0$. A level crossing occurs at $B = 2$ where the energy of the $m_z = -1$ state crosses with that of the $m_z = 0$ state. For a high energy system, the state would transition between $m_z = 0$ and $m_z = -1$ at $B = 2$. Another level crossing occurs at $B = 0$ where the energy of the $m_z = -1$ state crosses with that of the $m_z = 1$ state. A ground state phase transition would occur at $B = 0$.

1.3 The XY Model

Similar to the one-dimensional Ising model, the one-dimensional XY model describes spins on a one-dimensional lattice with interactions between neighboring sites. Each lattice site in the XY model has a full spin-$\frac{1}{2}$ degree of freedom, but spins interact with neighbors only with regards to their x and y-components. In this thesis, the XY model has a periodic boundary condition $\mathbf{S}_{N+1} = \mathbf{S}_1$ such that the one-dimensional chain of N lattice sites loop around like a ring. A schematic of the XY model can be seen in Figure 1.2. Furthermore, interactions of spins in the x and y-directions are described by the same coupling constant, J, to maintain rotational symmetry of each spin degree of freedom about the z-axis.

The Hamiltonian of the XY model is given by

$$\mathbf{H}_{XY} = -J \sum_{i=1}^{N} (\sigma_i^x \sigma_{i+1}^x + \sigma_i^y \sigma_{i+1}^y) \, . \tag{1.7}$$

Because the σ^x and σ^y matrices of the Hamiltonian do not commute (See Appendix A.1), the Hamiltonian in Eq. (1.7) cannot be easily diagonalized. The Jordan-Wigner transformation

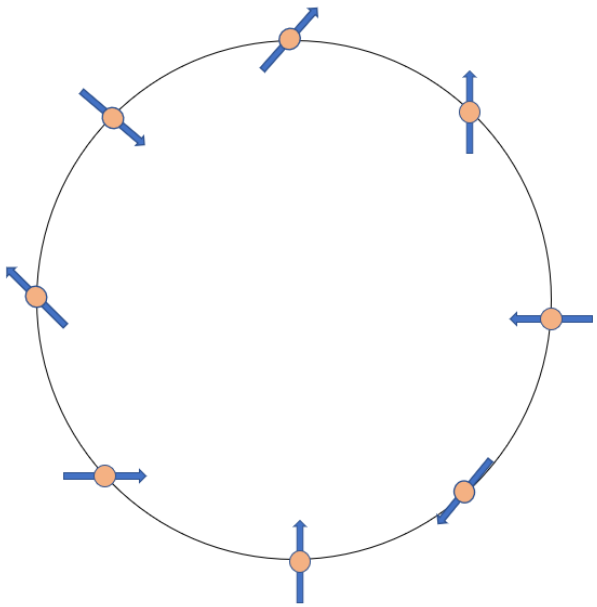

Figure 1.2: Schematic of an 8-site one-dimensional XY model with a periodic boundary condition. Spin-spin interactions in the x and y-directions occur between neighboring lattice sites.

can be used to diagonalize the Hamiltonian by mapping the spin operators of the XY Hamiltonian onto the fermionic creation and annihilation operators and transforming spin degrees of freedom into fermionic degrees of freedom. The resulting diagonalized Hamiltonian is given as

$$\mathbf{H}_{XY} = -\frac{J}{2}\sum_{i=1}^{N-1}(\mathbf{c}_i^\dagger \mathbf{c}_{i+1} + \mathbf{c}_{i+1}^\dagger \mathbf{c}_i) \tag{1.8}$$

(See Appendix A.2).

Level crossings can be induced in the XY model by adding a transverse magnetic field in the z-direction. The Hamiltonian of the XY model with a transverse field is given by

$$\mathbf{H}_{XY} = -J\sum_{i=1}^{N}(\sigma_i^x\sigma_{i+1}^x + \sigma_i^y\sigma_{i+1}^y) - B\sum_{i=1}^{N}\sigma_i^z \ . \tag{1.9}$$

Because the XY Hamiltonian and the $\mathbf{S}^z$ spin operator commute, m_z is a good quantum number for this model. For a zero-temperature system, a magnetic field creates level crossings that allow for phase transitions in the ground state. An example of level crossings in a 2-site

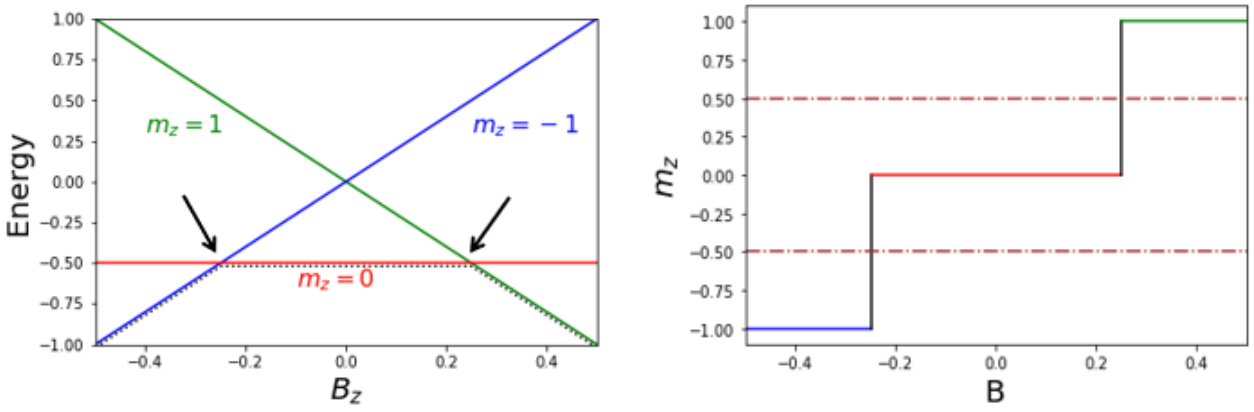

Figure 1.3: Left: Energies of a 2 site XY model over an evolving magnetic field with $J = 1$. A level crossing occurs at $B = -0.25$ where the energies of the $m_z = -1$ state crosses with that of the $m_z = 0$ state. Another level crossing occurs at $B = 0.25$ where the energies of the $m_z = 1$ state crosses with that of the $m_z = 0$ state.

Right: For a ground state system, m_z would transition sharply at $B = -0.25$ and $B = 0.25$. The halfway point between two values of m_z is taken as where the phase transition occurred.

system is illustrated in Figure 1.3.

However, the commutation relation between the XY Hamiltonian and the observable operator $\mathbf{S}^z$ means that different eigenstates of the system cannot couple (See Appendix A.3). Thus, the usual methods of measuring phase transitions, as will be explained in the next section, become impossible in the one-dimensional XY model, and alternatives will have to be introduced.

1.4 Adiabatic State Preparation

The adiabatic theorem states that a system remains in its initial state if a slow enough perturbation acts upon it [2]. Complex Hamiltonians can be solved by the adiabatic theorem through a method called adiabatic state preparation. In brief, an initial ground state with a simple Hamiltonian is prepared. Afterwards, the ground state is evolved adiabatically to the desired Hamiltonian. This method is powerful in quantum computing to solve a variety

of problems [3]. If the ground state of a system is always nondegenerate, that is there are no level crossings in the ground state, and the perturbation changes slow enough, then a system in the ground state is guaranteed to remain in the ground state.

For cases in which level crossings exist, the Landau-Zener formula provides an analytical tool for describing an adiabatically evolving state [4]. If the perturbation acting on the state changes with a linear velocity for a two state system, then the probability that the ground state transitions diabatically to the excited state is given by

$$P(|e\rangle) = e^{-2\pi\Delta^2/(\hbar v)} , \tag{1.10}$$

where Δ is half the distance between the eigenenergies of the avoided crossing, and v is the velocity of the perturbation. For example, if the magnetic field of some system is given as $B(t) = B_0 - vt$, then v would be used for velocity in Eq. (1.10). Δ can also be interpreted as the off-diagonal element of the Hamiltonian with respect to different eigenstates of the observable. In other words, Δ is a measure of the coupling between eigenstates. If the Hamiltonian is diagonal, then there is no coupling between eigenstates. The probability of a diabatic transition is highest when v is high or Δ is low. For eigenstates with no coupling, Δ goes to 0 and the probability of a diabatic transition goes to 1. Hence, in a system with level crossings in the ground state due to a lack of coupling between eigenstates, adiabatic state preparation cannot be immediately used to find the ground-state phase diagram. Figure 1.4 illustrates an avoided crossing between two states whose probability of a diabatic transition is given by the Landau-Zener formula.

Because different eigenstates of the XY Hamiltonian do not couple, the probability of adiabatic phase transitions in the ground state is 0. The direct method to find the ground state phase transitions would be to initialize an all up spin or all down spin state and adiabatically evolve the system in the ground state to find where m_z changes as B varies. For the XY Hamiltonian, this method fails. A prepared eigenstate would maintain the same

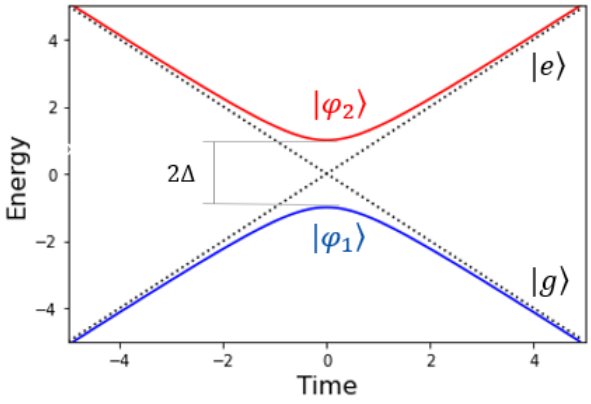

Figure 1.4: The Landau-Zener formula is an analytic solution to a system with a phase transition evolving under adiabatic phase evolution. The states $|e\rangle$ and $|g\rangle$ represent the excited and ground states, respectively, of a two state system. The states $|\phi_1\rangle$ and $|\phi_2\rangle$ represent adiabatic states that have an avoided crossing at time $t = 0$ due to a slow perturbation. At non-zero velocities of the time-evolving field, the probability that $|\phi_1\rangle$ diabatically transitions to $|e\rangle$ instead of remaining in $|g\rangle$ can be calculated using Eq. (1.10).

m_z quantum number as B varies and no phase transitions would occur. To induce coupling to perform adiabatic state preparation, the XY Hamiltonian needs to be modified to break its symmetry.

A simple way to modify the XY Hamiltonian is to add a small magnetic field in the x-direction, B_x. The transverse magnetic field will be referred to as B_z. The Hamiltonian with a symmetry-breaking magnetic field is given as

$$\mathbf{H}_{XY} = -J\sum_{i=1}^{N}(\sigma_i^x\sigma_{i+1}^x + \sigma_i^y\sigma_{i+1}^y) - B_z\sum_{i=1}^{N}\sigma_i^z - B_x\sum_{i=1}^{N}\sigma_i^x \,. \tag{1.11}$$

Because the new σ^x term in the Hamiltonian does not commute with the observable σ^z (see Appendix A.1), the new Hamiltonian allows for coupling between eigenstates. This project will use quantum computers to run adiabatic state preparation on the one-dimensional 2-site XY Hamiltonian with $J = 1$ and different values of B_x and record the transverse field magnitude at which a phase transition occurs. The data can then be extrapolated to $B_x = 0$ to find the exact phase transition of the ground state. Demonstrating the procedure in the 2-site system will serve as a proof-of-concept for calculations with larger-systems in the

future.

1.5 Magnetic Field Ramps

For adiabatic state preparation to succeed, the velocity of the magnetic field has to change slowly near where an adiabatic transition may occur. A ramp is the function for this velocity. A good ramp has to balance a small velocity near adiabatic transitions with a large enough velocity that the complete time-evolution can be done in reasonable time.

It has been shown that a local adiabatic ramp is an excellent choice to produce the least diabatic evolutions [5]. It is set up so as to have the same amount of diabatic excitation at each time step. For the XY model, given an initial transverse field magnitude B_0, the locally adiabatic ramp can be calculated from

$$t(B_z) = -\gamma \int_{B_0}^{B_z} \frac{dB_z'}{\Delta^2(B_z')} \,, \tag{1.12}$$

where Δ, or the instantaneous gap, is the energy difference between the first order and ground state of the XY Hamiltonian, and γ is the adiabacity parameter of the ramp. The adiabacity parameter can be changed to control the total evolution time of the system. γ must be larger than 1 to satisfy the locally adiabatic criterion; the larger the γ, the more adiabatic the ramp. Δ is smallest near adiabatic transitions, so $t(B_z)$ will change fastest at those points. $t(B_z)$ can be splined and inverted to derive a time-dependent magnetic field ramp $B_z(t)$. Near the level crossing, $B_z(t)$ will have a small velocity which is consistent for adiabatic phase transitions. The time-dependent XY Hamiltonian is now given by

$$\mathbf{H}_{XY}(t) = -J \sum_{i=1}^{N} (\sigma_i^x \sigma_{i+1}^x + \sigma_i^y \sigma_{i+1}^y) - B_z(t) \sum_{i=1}^{N} \sigma_i^z - B_x \sum_{i=1}^{N} \sigma_i^x \,. \tag{1.13}$$

The local adiabatic ramp has already been shown to be an effective adiabatic function in finding transitions in systems with spin-spin interactions. Its ability to keep the same level

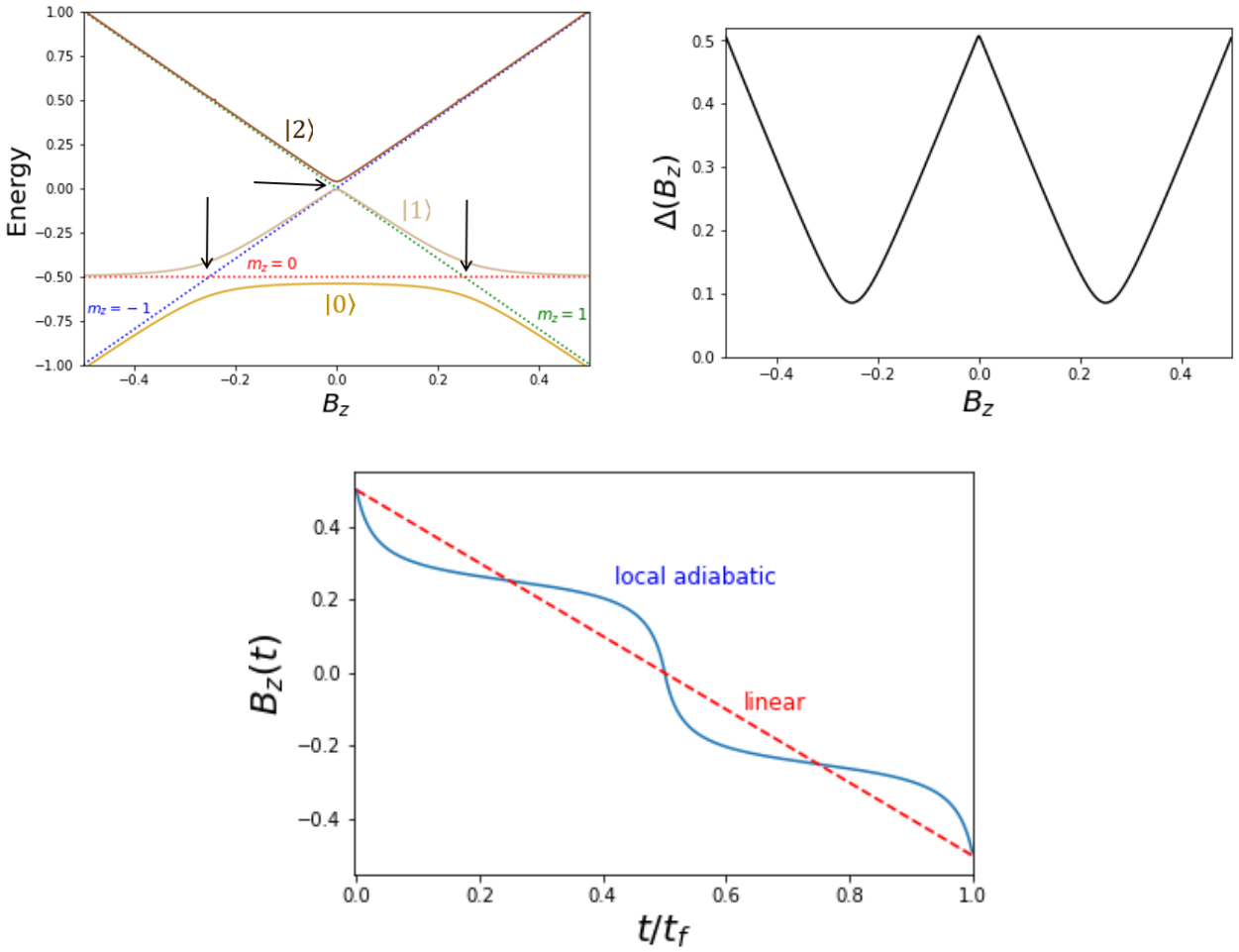

Figure 1.5: Top Left: The solid lines represent the eigenstates of the modified 2-site XY Hamiltonian with a small B_x field. The eigenstates of the XY Hamiltonian without a B_x field are shown in dotted lines. Because m_z is not longer a good quantum number for the new Hamiltonian, the quantum numbers refer only to the dotted lines. The $|0\rangle$ state of the new Hamiltonian can adiabatically evolve over the original eigenstates in the ground state. The solid black arrows point to avoided level crossings between the eigenstates of the new Hamiltonian. The energy difference between $|0\rangle$ and $|1\rangle$ is smallest at $B_z = -0.25$ and $B_z = 0.25$. A larger energy difference occurs between $|0\rangle$ and $|1\rangle$ at $B_z = 0$.

Top Right: Energy difference of the ground state and first excited state of the modified 2-site XY Hamiltonian with a small B_x field. $\Delta(B_z)$ is smallest at the avoided crossings of the ground state at $B_z = -0.25$ and $B_z = 0.25$.

Bottom: Comparison between a local adiabatic ramp and linear ramp for the modified 2-site XY Hamiltonian with a small B_x field. A spline was mapped over points calculated from Eq. (1.12) to derive the ramp $B_z(t)$. The local adiabatic ramp slows down at $B_z = -0.25$ and $B_z = 0.25$ to encourage adiabatic evolution but speeds up otherwise to decrease the time necessary for complete time-evolution. The linear ramp maintains a constant velocity, drastically increasing the diabatic excitation for the same total time run.

of diabatic excitations from the ground state for each time interval is the best one can do with a continuous ramp in finite time. Figure 1.5 shows how the energies of the eigenstates of the modified one-dimensional 2-site XY Hamiltonian with a nonzero B_x can be used to calculate a locally adiabatic ramp.

1.6 Quantum Computing

Recent developments in quantum computing has generated excitement among scientists on the possibility of solving problems infeasible on a classical computer. For example, some well-known properties of the Ising model have been successfully demonstrated in a quantum computer, both showing its proof-of-concept and offering exciting opportunities when quantum hardware matures [6]. Coincidentally, the Ising model, XY model, and similar statistical mechanics models have important ramifications on our understanding of quantum computing hardware itself [7][8].

A quantum computer uses qubits to represent quantum systems that are entangled or in superposition. Its ability to efficiently store quantum states and have unitary operators act on those states makes it superior to operations on a classical computer. Since the Hilbert space grows exponentially for more entangled states, conventional computers are constrained by space and time limitations when modeling large quantum systems. Currently, all calculations that can be done in quantum computers are capable of being replicated in classical computers because of technical difficulties in creating controlled quantum computing hardware. However, as quantum hardware evolves, scientists will be able to better understand solutions to a range of quantum mechanical problems. The milestone in which quantum computers can finally solve problems infeasible in a classical computer (due to time and space constraints) is called quantum advantage.

The phase transitions of the XY model for a few sites can be solved exactly in a classical computer by simulating adiabatic state preparation. However, the problem becomes

exponentially more difficult to solve as more lattice sites are added to the system, so much so that it would be infeasible to solve the problem on a classical computer when the number of lattice sites is larger than about 40. This project will create a circuit of the 2-site XY model and compare the results from a classical calculation with the experimental results from a quantum computer as a proof-of-concept for adiabatic evolution by breaking the symmetry of the XY Hamiltonian. Current quantum hardware can be used to solve the phase transitions of the XY model for only a few sites, but as quantum hardware becomes more robust, this method can be replicated for XY models with more sites.

Quantum computers use a universal quantum gate set to create circuits so that any logical gate can be reduced to a small set of operations. Usually, the universal gate set needs to be converted into an intrinsic, hardware-efficient gateset of the quantum hardware before the circuit can run. Currently, all systems that are modeled in a quantum computer must use unitary, reversible operations unless partial reset of qubits become more common in future hardware.

1.7 Unitary Decomposition

To replicate a time-evolving XY model in a quantum computer, the XY Hamiltonian must be transformed into a unitary operator, $\mathbf{U}_{XY}$, and evolved using the Trotter Approximation. The Trotter Approximation can be used to decompose a time-evolving operator from time t_0 to time t using a product of unitary terms to approximate the time-ordered product

$$\mathbf{U}(t, t_0) \approx e^{-i\mathbf{H}(t-\Delta t)\Delta t}\, e^{-i\mathbf{H}(t-2\Delta t)\Delta t} \ldots\, e^{-i\mathbf{H}(t_0)\Delta t}\,, \tag{1.14}$$

where Δt is a discrete time interval, and $\mathbf{H}(t)$ is the time-dependent nonunitary operator. Each unitary term is also called a Trotter step. Because each Trotter step is an unitary operator, it can be implemented as a set of unitary quantum gates. Essentially, the time evolution is broken down into discrete Trotter steps that approach the exact solution as

$\Delta t \to 0$.

The smaller the Δt, the more Trotter steps are required to implement the time-evolution, and the more complex the quantum circuit becomes. Current quantum hardware can perform calculations with good fidelity to only about 50 controlled-not operations, or $CNOT$ gates. Thus, the unitary operator has to approximate the exact solution well even when Δt is large.

Chapter 2

Methods

2.1 Decomposing the XY Hamiltonian

To calculate the ground state phase transition of the XY model, a magnetic field in the z-direction was added to induce phase transitions and a magnetic field in the x-direction was added to induce coupling between eigenstates. The complete XY Hamiltonian, as will be used for the remainder of the thesis, is given by

$$\mathbf{H}_{XY}(t) = \underbrace{-J\sum_{i=1}^{N}(\sigma_i^x\sigma_{i+1}^x + \sigma_i^y\sigma_{i+1}^y)}_{J\ comp.} \underbrace{- B_z(t)\sum_{i=1}^{N}\sigma_i^z}_{Bz\ comp.} \underbrace{- B_x\sum_{i=1}^{N}\sigma_i^x}_{Bx\ comp.}, \tag{2.1}$$

where each term will be referred to as the J component, B_z component, or B_x component. To simulate the XY Hamiltonian in a quantum computer, the time evolved Hamiltonian was decomposed into a set of unitary operators, and the time evolution was approximated using Trotter decomposition to produce

$$\mathbf{U}_{XY}(t, t_0) \approx e^{-i\mathbf{H}_{XY}(t-\Delta t)\Delta t}\ e^{-i\mathbf{H}_{XY}(t-2\Delta t)\Delta t} \ldots\ e^{-i\mathbf{H}_{XY}(t_0)\Delta t}\ . \tag{2.2}$$

Quantum circuits cannot implement noncommuting operators on a qubit at the same time. Because the XY Hamiltonian contains noncommuting elements, each Trotter step must also be decomposed. A direct method for decomposition could be

$$e^{-i\mathbf{H}_{XY}(t)\Delta t} \approx \underbrace{e^{-i\mathbf{H}_J\Delta t}}_{J\ comp.}\ \underbrace{e^{-i\mathbf{H}_{Bz}(t)\Delta t}}_{Bz\ comp.}\ \underbrace{e^{-i\mathbf{H}_{Bx}\Delta t}}_{Bx\ comp.}\,, \tag{2.3}$$

where each term in the XY Hamiltonian is transformed into a unitary operator.

However, the Heisenberg representation of the XY Hamiltonian can also be transformed into the interaction representation and decomposed in the interaction picture (See Appendix A.4). The XY Hamiltonian in the interaction representation is given by

$$\mathbf{V}_I(t) = \underbrace{-J\sum_i(\sigma_i^x\sigma_{i+1}^x + \sigma_i^y\sigma_{i+1}^y)}_{J\ comp.} \underbrace{- B_x\sum_i(cos\theta(t)\sigma_i^x + sin\theta(t)\sigma_i^y)}_{I\ comp.}\,, \tag{2.4}$$

where

$$\theta(t) = \int_0^t B_z(t')dt'\ . \tag{2.5}$$

Instead of the system evolving directly under a time-dependent B_z field, the system now evolves according to $\theta(t)$ with a time varying small field in the x-y plane. The interaction picture can be thought of as evolving the system in a rotating frame of reference given by $\theta(t)$. A single Trotter step in the interaction picture is given by

$$e^{-i\mathbf{V}_I(t)\Delta t} = \underbrace{e^{-i\mathbf{H}_J\Delta t}}_{J\ comp.}\underbrace{e^{-i\mathbf{H}_I(t)\Delta t}}_{I\ comp.}\ . \tag{2.6}$$

In this case, the interaction picture of the XY Hamiltonian holds two advantages over the Heisenberg picture. First, the I component of Eq. (2.6) can be thought of as a single rotation of a Bloch sphere along the axis pointing at the angle $\theta(t)$ in the XY plane with the magnitude of the rotation given by B_x. Whereas the Heisenberg picture required separate terms and separate gates for the B_z and B_x fields, as denoted by Eq. (2.3), the

interaction picture simplified two gates into one. Furthermore, as seen in Figure 2.1, the interaction picture performs well for large Δt. This could be due to the interaction picture being only dependent on the small B_x of the system and not a time-dependent B_z. Due to quantum computing hardware limitations, the ability to accurately time-evolve the system with a small number of Trotter steps is a valuable property. Thus, the interaction picture of the Hamiltonian was implemented as a quantum circuit to find the one-dimensional 2-site XY model phase transitions.

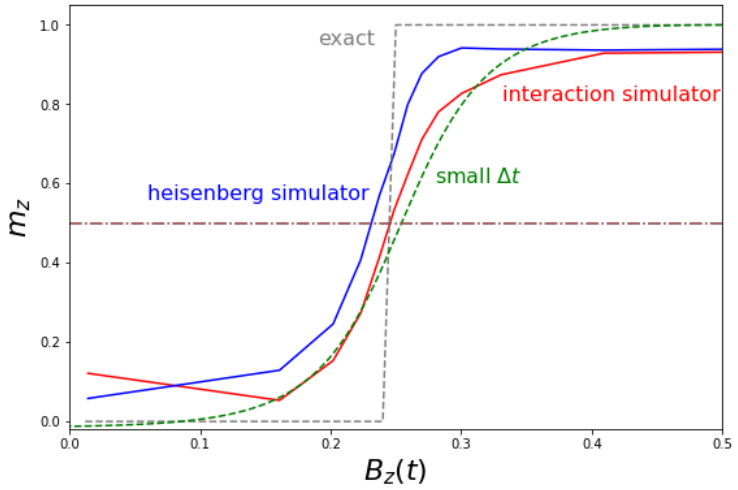

Figure 2.1: The eigenvalue of the XY Hamiltonian was measured over a time-evolving B_z field for a quantum circuit simulator implementing the Heisenberg picture, shown in the blue line, and for a simulator implementing the interaction picture, shown in the red line. The simulation evolved from $B_0 = 0.5$ to $B_f = 0$. The total time-evolution for both circuits required 13 Trotter steps with large Δt. The discrete transition for the exact solution to the XY Hamiltonian is shown in gray, and the approximate transition for the modified Hamiltonian with a nonzero B_x decomposed into Trotter steps with small Δt is shown in green. Note that the green and red curves are similar.

2.2 Local Adiabatic Ramp

A local adiabatic ramp was used to vary the B_z field of the XY Hamiltonian. To find the locally adiabatic ramp with parameters B_0 and γ, the XY Hamiltonian as a function of B_z was diagonalized as the magnetic field evolved from $B_z = B_0$ to $B_z = B_f$. Given B_0, $\Delta(B_z)$

was calculated from equally spaced intervals of B_z between B_0 and B_f. Using that result, t_f was calculated using Eq. (1.12) to yield times as a function of B_z. An Akima spline, a shape-preserving spline, was then used to transform $t(B_z)$ to the ramp $B_z(t)$.

2.3 Quantum Circuit

Each term of the unitary Trotter step in the interaction representation for the 2-site XY Hamiltonian was transformed into unitary gates separately. The J component of Eq. (2.6) was decomposed into a quantum circuit with two controlled-NOT gates [9][10]. The circuit was constructed as

$e^{-i\mathbf{H}_J\Delta t} =$ 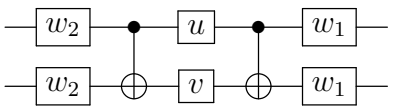

, (2.7)

where

$$w_1 = \frac{\mathbb{1} - i\sigma^x}{\sqrt{2}} \qquad w_2 = w_1^{-1} \tag{2.8}$$

$$u = e^{-iJ\sigma^x\Delta t} \qquad v = e^{iJ\sigma^z\Delta t}, \tag{2.9}$$

$\mathbb{1}$ represents the 2×2 identity operator, and w_2 is the conjugate transpose of w_1. In essence, the unitary Trotter step has been decomposed into a product of matrices. A quantum circuit is able to carry out each product operation successively through quantum gates [11]. Each single-qubit rotation gate is a 2×2 matrix. The $CNOT$ gate is a 4×4 matrix given by

 $= \begin{pmatrix} 1 & 0 & 0 & 0 \\ 0 & 1 & 0 & 0 \\ 0 & 0 & 0 & 1 \\ 0 & 0 & 1 & 0 \end{pmatrix}$. (2.10)

The product state of the 2-site system, a 1×4 matrix, enters the quantum circuit and undergoes the matrix operations through each unitary quantum gate. Matrix multiplication of the unitary gates are carried out from right to left in the circuit. The circuit can also be represented as a 4×4 matrix that performs the intended operation. The two qubits in the circuit begin in the Bell basis, a set of two-particle quantum states that have maximum entanglement. The w_2 and first $CNOT$ gates map the qubits from their original Bell basis to a convenient product basis, the u_2 and v_2 gates perform the appropriate rotations on either qubits in the product basis, and the last $CNOT$ and w_1 gates map back to the original Bell basis.

The I term of Eq. (2.6) was transformed into a single unitary gate. Using the identity $e^{i\vec{v}\cdot\vec{\sigma}} = cos|v|\mathbb{1} + i\frac{\vec{v}\cdot\vec{\sigma}}{|v|}sin|v|$, for a single qubit,

$$e^{-iB_x\Delta t(cos\theta(t)\sigma_i^x + sin\theta(t)\sigma_i^y)} = cos(B_x\Delta t)\mathbb{1} + isin(B_x\Delta t)[cos(\theta)\sigma^x + sin(\theta)\sigma^y] \; . \tag{2.11}$$

The result of Eq. (2.11) was transformed into the basic unitary quantum gate

$$e^{-i\mathbf{H}_I(t)\Delta t} = \begin{array}{l} —\boxed{U(B_x\Delta t, \theta + \pi/2, -\theta - \pi/2)}— \\ —\boxed{U(B_x\Delta t, \theta + \pi/2, -\theta - \pi/2)}— \end{array} , \tag{2.12}$$

where the U gate represents a generalized single-qubit rotation. In IBM Quantum systems, all single unitary gates can be decomposed into U gates. An U gate is equivalent to rotations about the z-axis with the RZ gate and rotations about the x-axis with the RX gate using 3 angles,

$$U(\theta, \phi, \lambda) = RZ(\phi - \frac{\pi}{2})RX(\frac{\pi}{2})RZ(\pi - \theta)RX(\frac{\pi}{2})RZ(\lambda - \frac{\pi}{2}) \; . \tag{2.13}$$

The total quantum circuit in the interaction representation for a single Trotter step was

implemented as

$$e^{-i\mathbf{V}_I(t)\Delta t} = \quad (2.14)$$

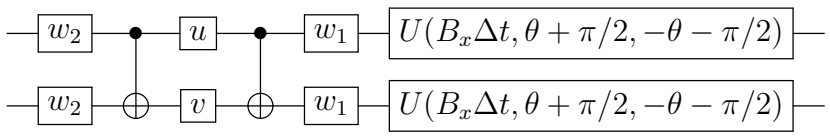

For each Trotter step, two $CNOT$ gates were required.

2.4 Determining Parameters

Before running the XY Hamiltonian on quantum computers, suitable parameters had to be chosen for the variables in the model. The different possible parameters for this experiment are shown in Table 2.1. The XY Hamiltonian was evolved in simulated quantum computers to choose the best variables to input for real quantum computers. The parameters were chosen such that the total time-evolution needed only around 25 Trotter steps (around 50 $CNOT$ gates), but was long enough such that a phase transition could be observed. Because of the difficulty in observing both phase transitions of the 2-site XY Model with only 25 Trotter steps for time-evolution, the phase transition from $m_z = -1$ to $m_z = 0$ and from $m_z = 1$ to $m_z = 0$ were calculated separately. The former transition will be referred to as the negative transition, and the latter as the positive transition. Thus, the adiabatic ramp only needed to be calculated from B_0 to $B_f = 0$ for both cases.

Table 2.1: Parameters in Evolving the XY Hamiltonian

J	Coupling constant of the XY Hamiltonian
B_x	Magnitude of magnetic field in the x direction
$B_z(t_0)$	Initial magnitude of magnetic field in the z direction
Δt	Size of discrete Trotter steps
γ	Adiabacity parameter of local adiabatic ramp

To find the parameters, J was set to 1 for simplicity. Furthermore, $B_z(t_0)$ was set

to $B_0 = 2$ and $B_0 = -2$ for the positive and negative transitions, respectively, so that the initial ground state began far from the adiabatic transition point at $B_z = 0.25$. The three sets of parameters chosen to run on quantum computers were

1. $B_x = 0.03$, $\Delta t = 2$, $\gamma = 3$, Trotter steps $= 26$

2. $B_x = 0.05$, $\Delta t = 1.6$, $\gamma = 4$, Trotter steps $= 25$

3. $B_x = 0.1$, $\Delta t = 0.9$, $\gamma = 5$, Trotter steps $= 25$

The simulator results of those parameters are illustrated in Figure 2.2.

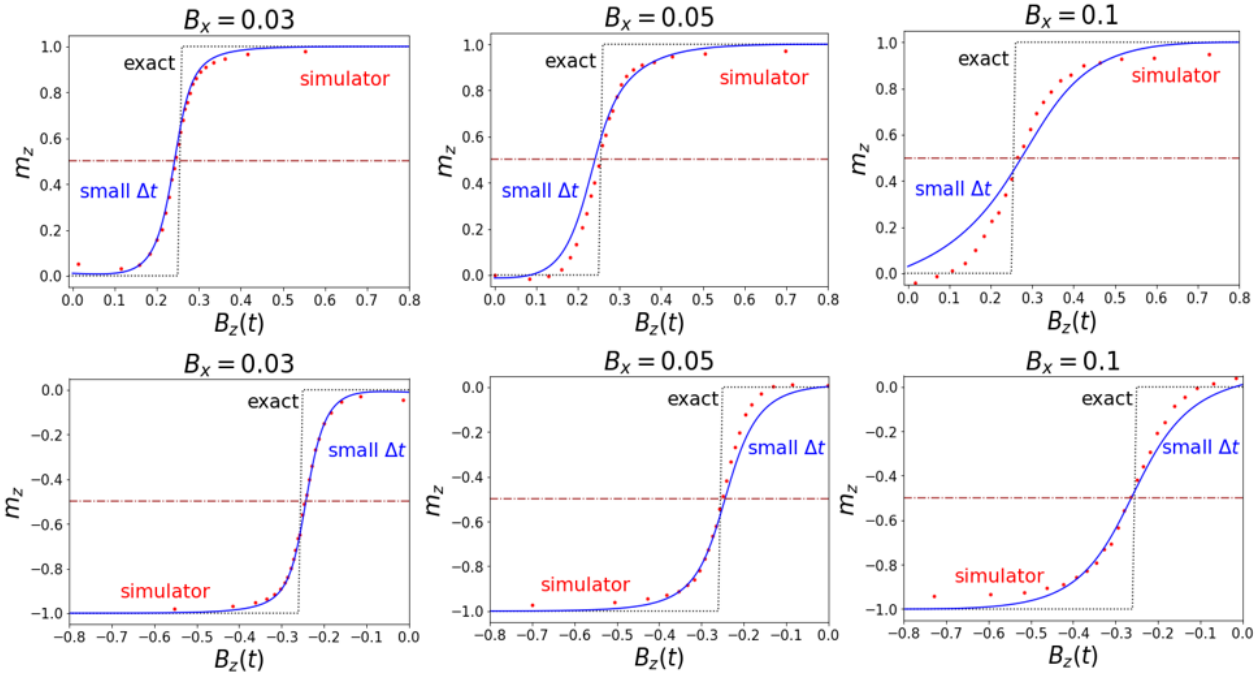

Figure 2.2: Data from quantum simulators, represented by red dots, for the positive (Top) and negative transitions (Bottom) evolved with the XY Hamiltonian specified with the three parameters are compared to the evolution in a quantum simulator for systems with those parameters but with small Δt, represented by blue lines, and the exact solution with $B_x = 0$, represented by a gray dotted lines. The simulator data and exact solution crosses the halfway point for m_z at approximately the same B_z.

2.5 Running a Job on IBM Quantum Experience

Due to its low queue times and high qubit fidelity, IBM's 'ibmq_santiago' machine was chosen for evolving the 2-site XY Hamiltonian. Before running the full time-evolution on the machine, the results from running 5 Trotter steps of the $B_x = 0.03$ parameters on each pair of qubits were measured. The pair of qubits with the lowest noise was chosen to be the physical qubits on which the quantum circuits would be run.

Six total jobs were performed on 'ibmq_santiago': 3 sets of chosen parameters for both negative and positive transitions. For a job with N Trotter steps for the full time-evolution, a measurement of m_z was taken after the circuit was allowed to evolve for 0 steps, 1 step, 2 steps, and so on to N steps.

To calculate the exact phase transitions of the one-dimensional 2-site XY Model, the B_z at which the ground state crosses the halfway point between two quantum numbers was plotted against the magnitude of B_x. The data was then fit and extrapolated to $B_x = 0$. To illustrate this idea, an example using the exact solutions of the modified XY Hamiltonian with nonzero B_x is provided in Figure 2.3.

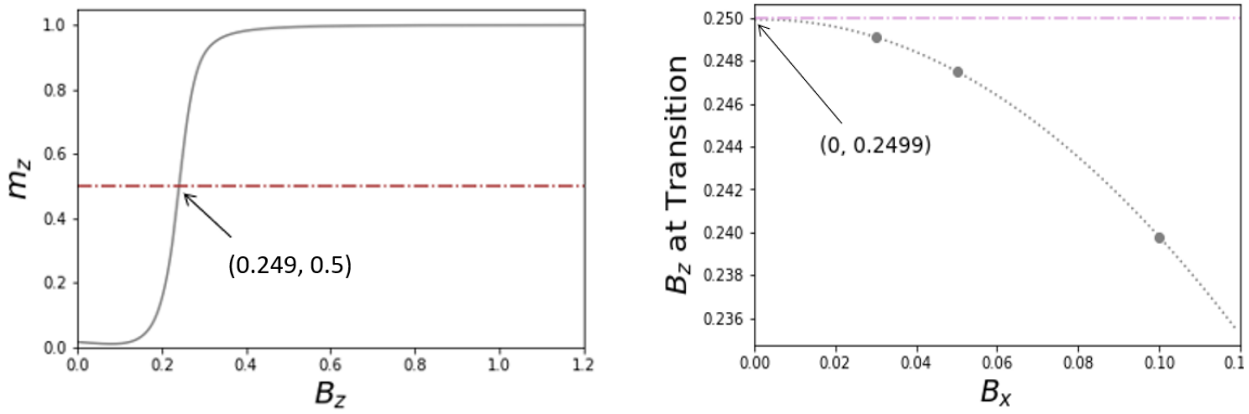

Figure 2.3: Left: The exact positive phase transition for the modified XY Hamiltonian with $B_x = 0.03$ was calculated on a conventional computer. The $m_z = 1$ state crosses $m_z = 0.5$ at $B_z = 0.249$.

Right: The phase transition at various B_z for the modified XY Hamiltonian with $B_x = 0.03$, $B_x = 0.05$, and $B_x = 0.1$ were fit to a quadratic curve. The curve was extrapolated to find that the phase transition for $B_x = 0$ occurs at $B_z = 0.2499$. The exact transition is known to occur at $B_z = 0.25$.

Chapter 3

Results and Discussion

The raw data obtained from the quantum computers show phase transitions close to the predicted B_z as shown in Figure 3.1.

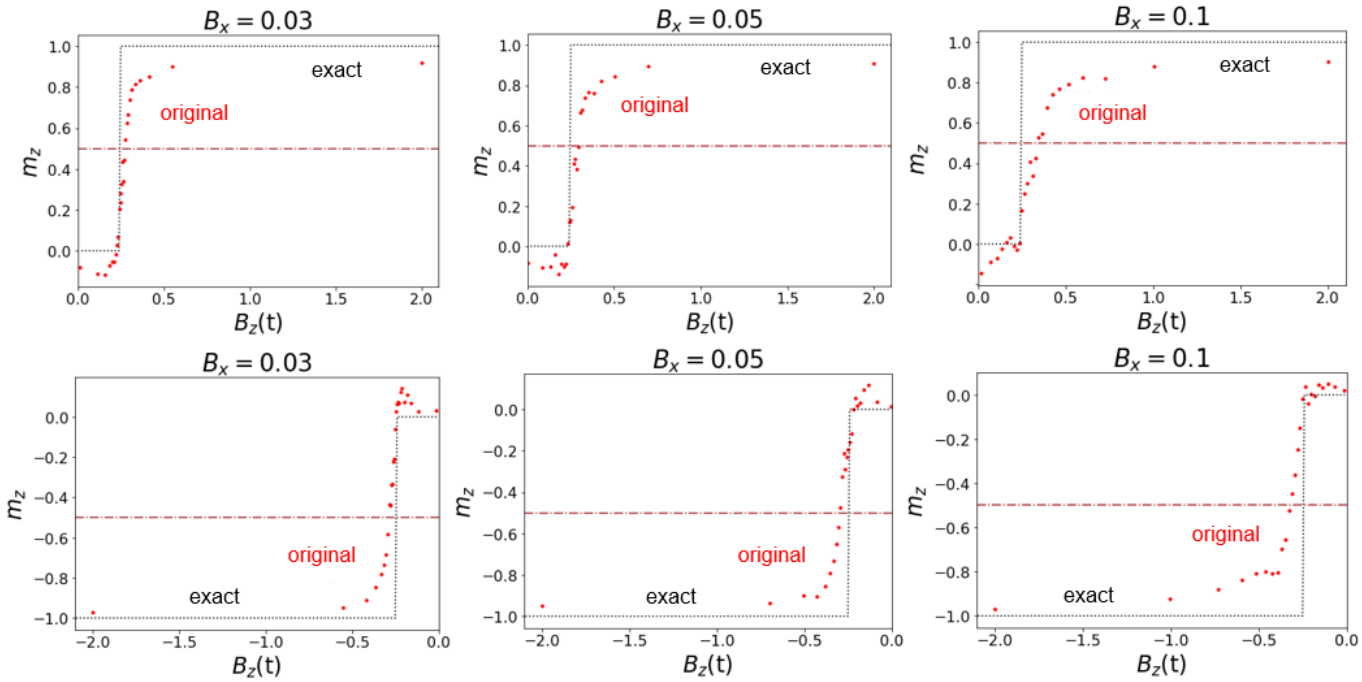

Figure 3.1: The XY Hamiltonian was evolved in a quantum computer for both positive (Top) and negative (Bottom) transitions for each set of parameters. The gray dotted line shows the exact solution for each case, and the red dots are the results from the quantum computer.

To correct for noise in the quantum hardware, the original data was either translated or scaled so that the initial measurements match the expected m_z of the initialized state.

Figure 3.2 shows the process for translating or scaling the data for the positive transition with the $B_x = 0.03$ parameter.

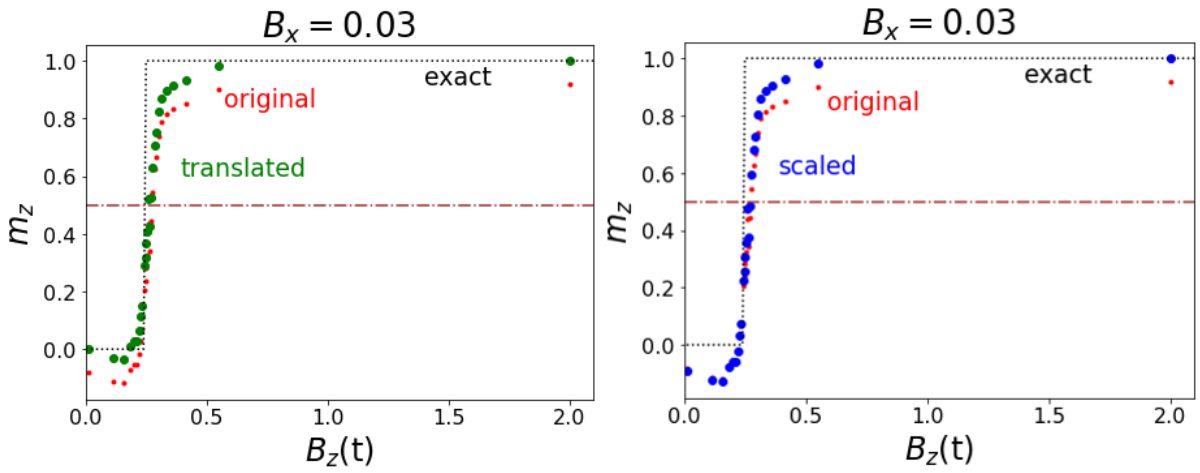

Figure 3.2: The original data for the positive transition for the case $B_x = 0.03$ is translated (left) or scaled (right) so that the initial eigenvalue begins at the expected $m_z = 1$.

To find the value at which the data crosses $m_z = 0.5$ for the positive transition and $m_z = -0.5$ for the negative transition, linear regression was run on the translated or scaled data. Linear regression was run for the 2, 4, 6, and 8 points closest to the transition line. Figure 3.3 shows the results of running regression on the scaled data for the positive transition for the case $B_x = 0.03$. The scaled and translated data for the case $B_x = 0.03$ match the exact solution well.

For a given positive or negative transition, scaled or translated data, and number of regression points, the B_z at which a phase transition occurred as a function of B_x was plotted and fit. The fits were extrapolated to $B_x = 0$ to find the exact phase transitions of the XY model. Figures 3.4 and 3.5 show the results for the positive transition. Figures 3.6 and 3.7 show the results for the negative transition. Tables 3.1 and 3.2 show the results of the fit extrapolated to $B_x = 0$ for the positive and negative transitions, respectively.

The extrapolated data agrees well with the known positive phase transition at $B_z = 0.25$ and the negative phase transition at $B_z = -0.25$. The data for the positive phase transition performed better than that for the negative transition. In fact, the 2 point regression

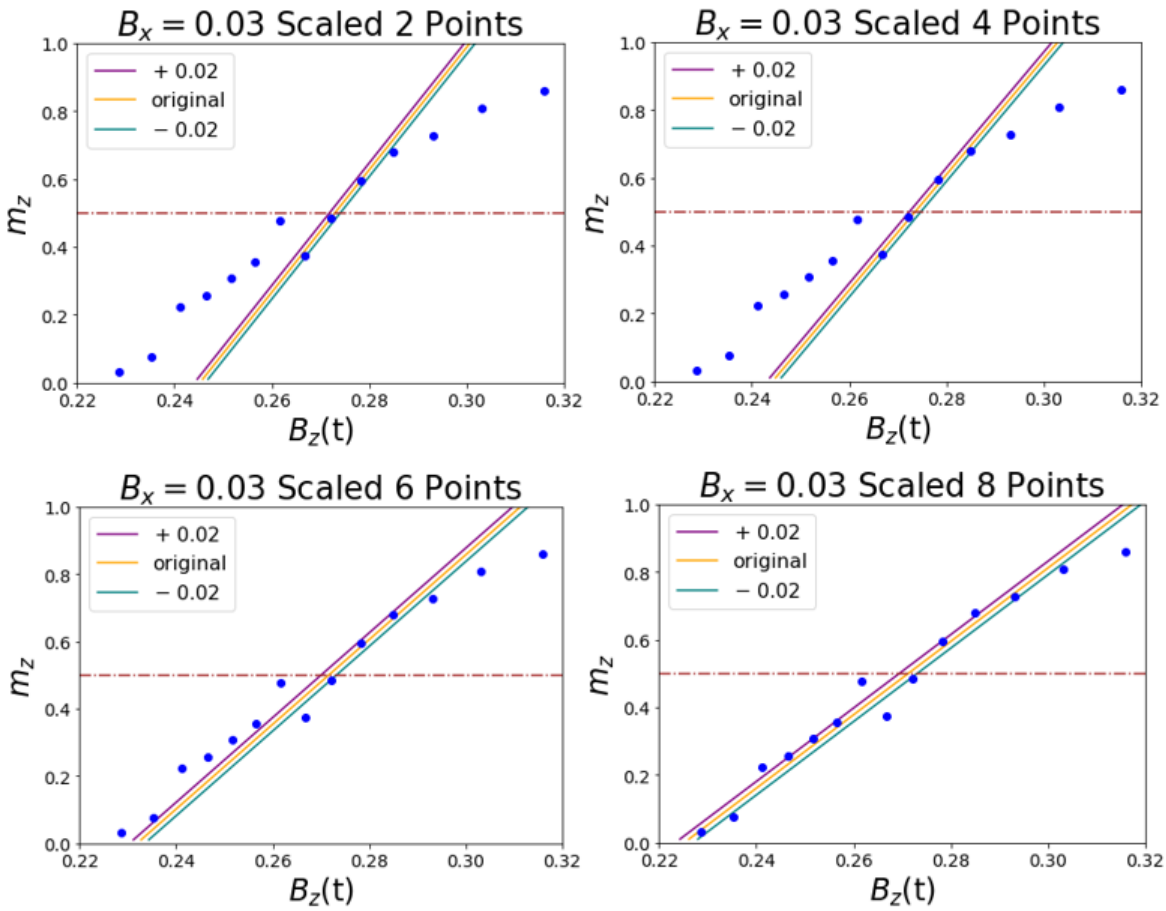

Figure 3.3: Regressions of the 2, 4, 6, and 8 points closest to the transition line at $m_z = 0.5$ were performed for the scaled data of the positive transition for the case $B_x = 0.03$. Each measurement was recorded as the average of 5000 shots in the quantum computer. The lines "+0.02" and "-0.02" correspond to the uncertainty from the average for each point. The uncertainty would be proportional to $\frac{1}{\sqrt{5000}}$, so 0.02 was chosen as the more conservative error.

of both the translated and scaled data for the positive transition matched the exact solution to three significant digits. The error in the experimentally calculated negative transition could have been exacerbated by the quadratic fits increasing in slope close to $B_x = 0$ instead of flattening out. Moreoever, the extrapolation from the regressions with 2 and 4 points calculated the negative phase transition the best. Regressions with fewer points yielded better results overall. However, for an accurate assessment of the error due to noise in the quantum computer, statistical errors, etc., more investigation is required.

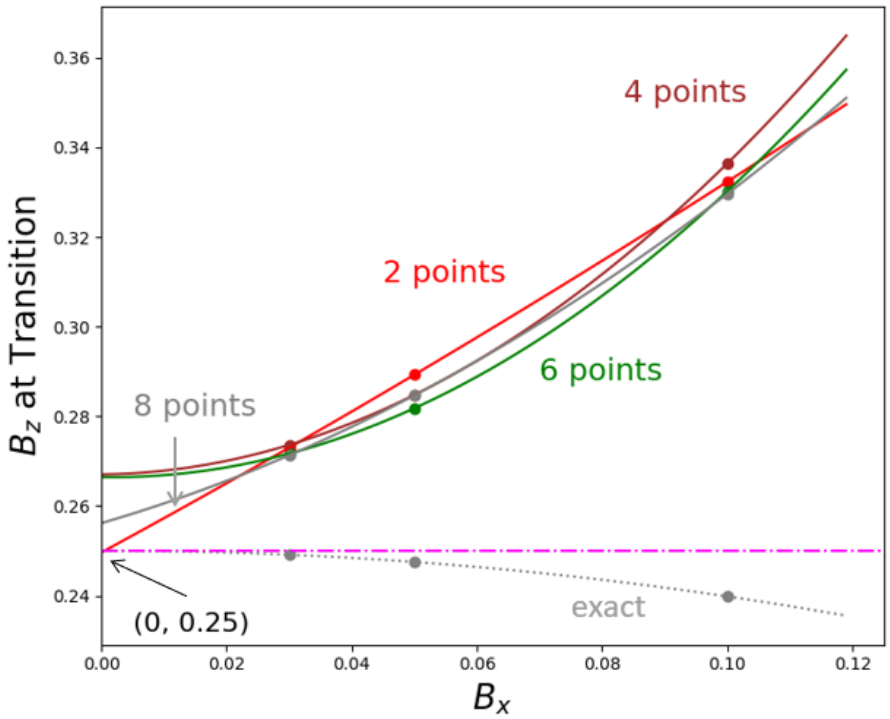

Figure 3.4: Quadratic fits of B_z at transition versus XY Hamiltonians with different values of B_x were done on regression results with various number of scaled data points. The fits were extrapolated to $B_x = 0$ to calculate the positive transition. The gray line shows extrapolating from the exact solutions of the modified XY Hamiltonian with various B_x.

Table 3.1: Extrapolating to $B_x = 0$ to Calculate the Positive Phase Transition

	Translated Data (B_x)	Scaled Data (B_x)
2 points	0.250	0.250
4 points	0.252	0.267
6 points	0.262	0.266
8 points	0.252	0.256

Table 3.2: Extrapolating to $B_x = 0$ to Calculate the Negative Phase Transition

	Translated Data (B_x)	Scaled Data (B_x)
2 points	-0.241	-0.245
4 points	-0.242	-0.244
6 points	-0.238	-0.239
8 points	-0.239	-0.239

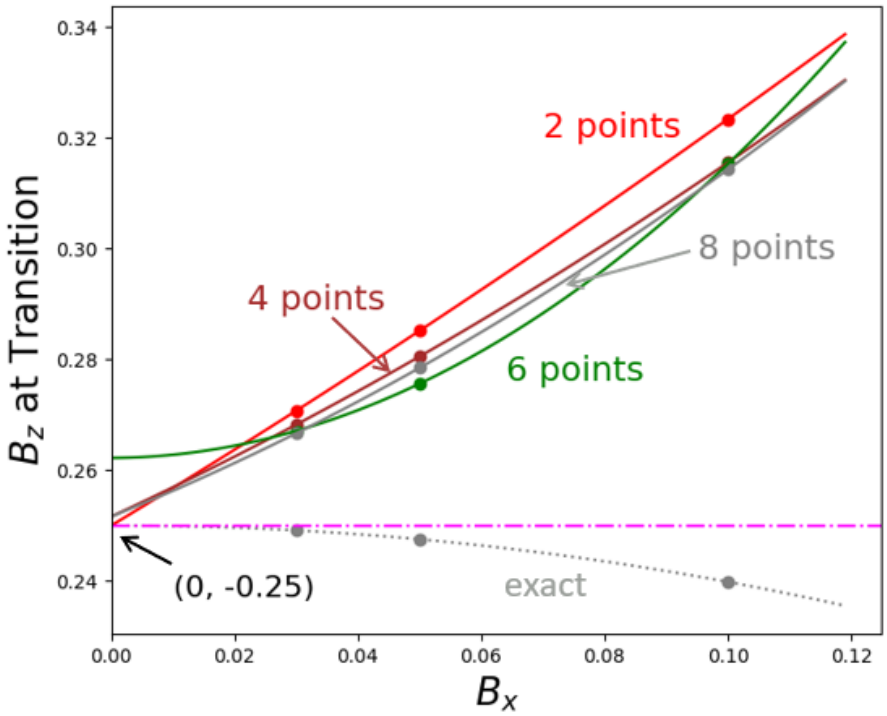

Figure 3.5: Quadratic fits of B_z at transition versus XY Hamiltonians with different values of B_x were done on regression results with various number of translated data points. The fits were extrapolated to $B_x = 0$ to calculate the positive transition. The gray line shows extrapolating from the exact solutions of the modified XY Hamiltonian with various B_x.

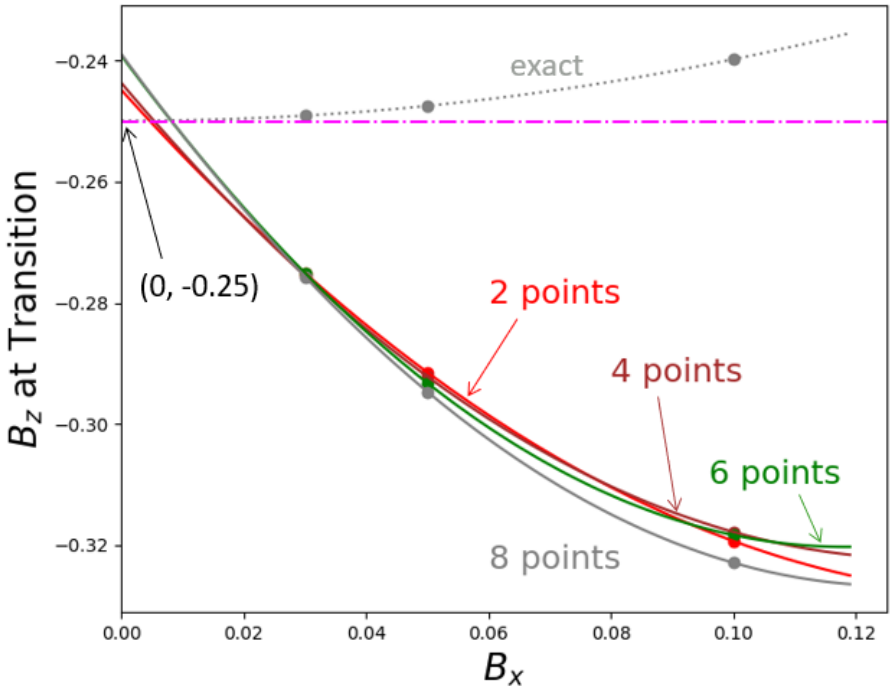

Figure 3.6: Quadratic fits of B_z at transition versus XY Hamiltonians with different values of B_x were done on regression results with various number of scaled data points. The fits were extrapolated to $B_x = 0$ to calculate the negative transition. The gray line shows extrapolating from the exact solutions of the modified XY Hamiltonian with various B_x.

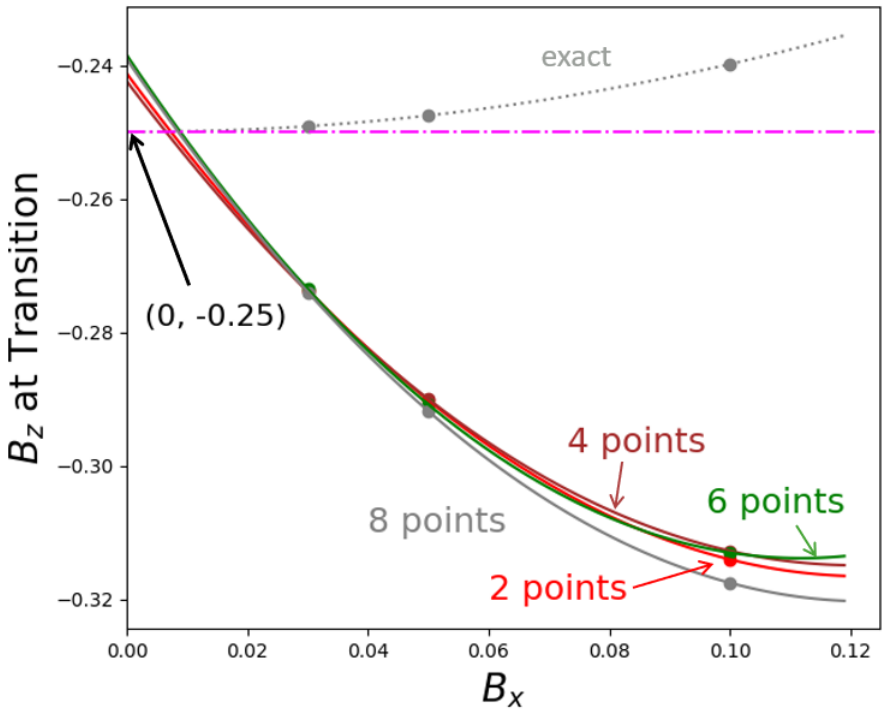

Figure 3.7: Quadratic fits of B_z at transition versus XY Hamiltonians with different values of B_x were done on regression results with various number of translated data points. The fits were extrapolated to $B_x = 0$ to calculate the negative transition. The gray line shows extrapolating from the exact solutions of the modified XY Hamiltonian with various B_x.

Chapter 4

Conclusion and Outlook

Given the unreliability of current quantum computers and the limitations of time evolution, the results of this thesis were encouraging. This thesis showed that for a Hamiltonian with eigenstates that cannot couple, breaking the symmetry by adding an additional magnetic field is an effective method for calculating its ground state phase transitions. Furthermore, extrapolating experimental results from a quantum computer is an accurate tool to calculate exact solutions in the one-dimensional 2-site XY model.

The method used in this thesis can easily be converted to find ground-state phase transitions for larger systems. The theory remains the same, and all but the instructions for the quantum circuit would change. Because the J component in Eq. (2.6) cannot be decomposed conveniently into unitary gates for larger systems, the 2-site circuit for the J component would be performed on nearest neighbors. For example, a 4-site system would carry out the J component circuit in Eq. (2.7) between sites 0 and 1, sites 1 and 2, sites 2 and 3, and sites 3 and 0. The I component of Eq. (2.6) can still be implemented as described in this thesis. For a systems with N sites, each Trotter step would contain $2N$ $CNOT$ gates per Trotter step.

The larger number of $CNOT$ gates per Trotter step limits the total number of Trotter steps that can be implemented in a quantum computer. Though time-evolution of the XY

model for 3 and 4-site systems work well in quantum computer simulators, the measurements are too noisy when evolved in a real quantum computer. A few attempts at extracting results for larger systems from a quantum computer have been unsuccessful. Figure 4.1 shows results from doing time-evolution for the 3-site one-dimensional XY Model in a quantum computer. The results are very poor and does not compare well with the known phase transitions of the model. Thus, current quantum hardware remains too noisy for time-evolution of more than two qubits for the XY Model.

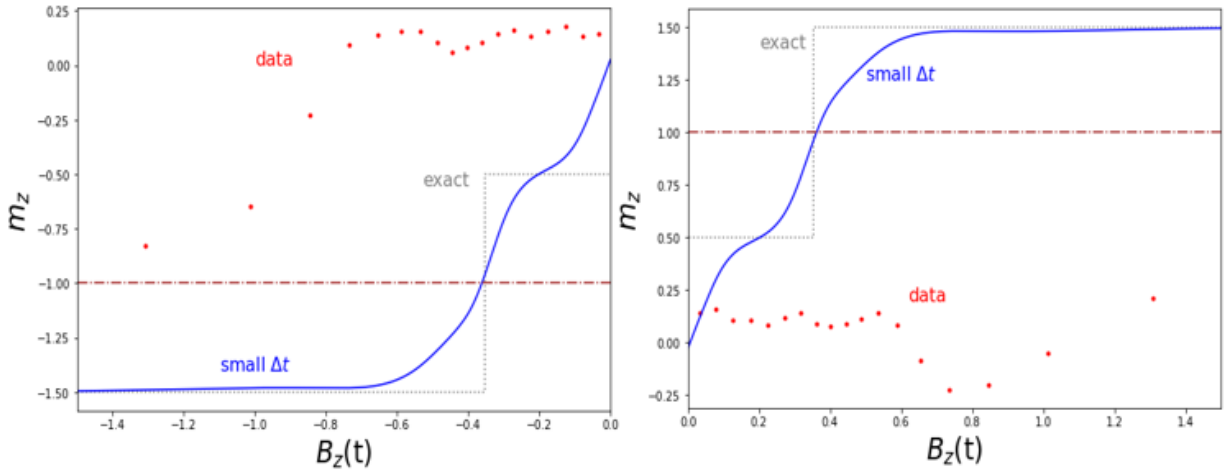

Figure 4.1: The 3-site one-dimensional XY Model with a $B_x = 0.2$ was evolved in a quantum computer for a range of negative B_z values (Right) and positive B_z value (Left). Both cases were evolved over a total time-evolution of 19 Trotter steps and 57 $CNOT$ gates. The results from the quantum computer, shown in red dots, compare poorly to the exact solution with $B_x = 0$ for the 3-site model, shown in the gray dotted line, and the quantum simulations of the XY Hamiltonian with $B_x = 0.2$ and small Δt, shown in the blue line.

As quantum hardware evolves, more robust calculations will hopefully soon be possible. When quantum advantage becomes widely available in quantum computers, the ground state phase transitions of new systems could be found quickly using the symmetry breaking and adiabatic state preparation described in this thesis. Furthermore, adiabatic phase transition could be carried out on systems whose eigenstates of the Hamiltonian are not coupled by explicitly breaking their symmetry to prepare ground states important for solving other problems. This work could be used to allow for adiabatic state preparation for a class of systems that was previously not possible.

Appendix A

Supplemental Proofs and Examples

A.1 Commutation Relation of Pauli Matrices

The Pauli spin matrices are expressed as

$$\sigma^x = \begin{pmatrix} 0 & 1 \\ 1 & 0 \end{pmatrix} \quad \sigma^y = \begin{pmatrix} 0 & -i \\ i & 0 \end{pmatrix} \quad \sigma^z = \begin{pmatrix} 1 & 0 \\ 0 & -1 \end{pmatrix} \tag{A.1}$$

The matrices have the commutation relation

$$[\sigma^a, \sigma^b] = 2i\epsilon_{abc}\sigma_c \ , \tag{A.2}$$

and the anticommutation relation

$$\{\sigma^a, \sigma^b\} = 2\delta_{ab}I \ . \tag{A.3}$$

A.2 Fermionic Representation of the XY Model

The XY Hamiltonian can be expressed as

$$\mathbf{H}_{XY} = -J \sum_{i=1}^{N} (\sigma_i^x \sigma_{i+1}^x + \sigma_i^y \sigma_{i+1}^y) \ . \tag{A.4}$$

Replacing $\sigma_i^x = \frac{1}{2}(\sigma_i^+ + \sigma_i^-)$ and $\sigma_i^y = \frac{1}{2i}(\sigma_i^+ - \sigma_i^-)$, where σ_i^+ and σ_i^- are the raising and lowering operators, respectively, into Eq. (A.4),

$$\mathbf{H}_{XY} = -\frac{J}{2} \sum_{i=1}^{N} (\sigma_i^+ \sigma_{i+1}^- + \sigma_i^- \sigma_{i+1}^+) \ . \tag{A.5}$$

To diagonize the Hamiltonian, let's define the fermionic creation and annihilation operators

$$\mathbf{c}_i^\dagger = e^{-i\frac{\pi}{2}\sum_{j=1}^{i-1}\sigma_j^z} \frac{\sigma_i^+}{2} \ , \tag{A.6}$$

$$\mathbf{c}_i = e^{i\frac{\pi}{2}\sum_{j=1}^{i-1}\sigma_j^z} \frac{\sigma_i^-}{2} \ . \tag{A.7}$$

The fermionic operators are so called because they anticommute (thus satisfying the Pauli exclusion principle), and states made out of creation operators acting on a vacuum state are always antisymmetric when two particles are exchanged.

$$\{\mathbf{c}_i, \mathbf{c}_j\} = 0 \longrightarrow (\mathbf{c}_i^\dagger)^2 = 0 \tag{A.8}$$

$$\mathbf{c}_2^\dagger \mathbf{c}_1^\dagger \mathbf{c}_3^\dagger |0\rangle = |213\rangle = -|123\rangle \tag{A.9}$$

The fermionic operators can be inverted to

$$\sigma_i^+ = e^{i\pi\sum_{j=1}^{i-1}\mathbf{n}_j} \mathbf{c}_i^\dagger \ , \tag{A.10}$$

$$\sigma_i^- = \mathbf{c}_i e^{-i\pi\sum_{j=1}^{i-1}\mathbf{n}_j} \ , \tag{A.11}$$

where $\mathbf{n}_i = \mathbf{c}_i^\dagger \mathbf{c}_i$ is the fermion number operator which counts the number of fermions on lattice site i. Now, let's substitute Eqs. (A.10) and (A.11) into Eq. (A.5).

$$\sigma_i^+ \sigma_{i+1}^- + \sigma_i^- \sigma_{i+1}^+ = e^{i\pi\sum_{j=1}^{i-1}\mathbf{n}_j} \mathbf{c}_i^\dagger \mathbf{c}_{i+1} e^{-i\pi\sum_{k=1}^{i}\mathbf{n}_k} + \mathbf{c}_i e^{-i\pi\sum_{j=1}^{i-1}\mathbf{n}_j} e^{i\pi\sum_{k=1}^{i}\mathbf{n}_k} \mathbf{c}_{i+1}^\dagger \tag{A.12}$$

$$= \mathbf{c}_i^\dagger e^{-i\pi\mathbf{n}_i} \mathbf{c}_{i+1} + \mathbf{c}_i e^{i\pi\mathbf{n}_i} \mathbf{c}_{i+1}^\dagger \ . \tag{A.13}$$

We can prove that $\mathbf{n}_i^2 = \mathbf{n}_i$ using $(\mathbf{c}_i^\dagger)^2 = 0$ and $\{\mathbf{c}_i, \mathbf{c}_j^\dagger\} = \delta_{ij}$,

$$\mathbf{c}_i^\dagger \mathbf{c}_i \mathbf{c}_i^\dagger \mathbf{c}_i = \mathbf{c}_i^\dagger \mathbf{c}_i \mathbf{c}_i^\dagger \mathbf{c}_i + \mathbf{c}_i^\dagger \mathbf{c}_i^\dagger \mathbf{c}_i \mathbf{c}_i = \mathbf{c}_i^\dagger \{\mathbf{c}_i, \mathbf{c}_i^\dagger\} \mathbf{c}_i = \mathbf{c}_i^\dagger \mathbf{c}_i \ . \tag{A.14}$$

Furthermore,

$$e^{i\theta \mathbf{n}_i} = 1 + i\theta \mathbf{n}_i + \frac{(i\theta \mathbf{n}_i)^2}{2!} + \frac{(i\theta \mathbf{n}_i)^3}{3!} + ... = 1 + (e^{i\theta} - 1)\mathbf{n}_1 \ . \tag{A.15}$$

For $\theta = \pi$,

$$e^{i\pi \mathbf{n}_i} = 1 - 2\mathbf{n}_i \ . \tag{A.16}$$

Continuing Eq. (A.13),

$$\mathbf{c}_i^\dagger e^{-i\pi \mathbf{n}_i} = \mathbf{c}_i^\dagger (1 - 2\mathbf{n}_i) = \mathbf{c}_i^\dagger \tag{A.17}$$

$$\mathbf{c}_i e^{i\pi \mathbf{n}_i} = \mathbf{c}_i (1 - 2\mathbf{n}_i) = \mathbf{c}_i - 2\mathbf{c}_i \mathbf{c}_i^\dagger \mathbf{c}_i = \mathbf{c}_i - 2\{\mathbf{c}_i, \mathbf{c}_i^\dagger\}\mathbf{c}_i = -\mathbf{c}_i \tag{A.18}$$

$$\sigma_i^+ \sigma_{i+1}^- + \sigma_i^- \sigma_{i+1}^+ = \mathbf{c}_i^\dagger \mathbf{c}_{i+1} - \mathbf{c}_i \mathbf{c}_{i+1}^\dagger = \mathbf{c}_i^\dagger \mathbf{c}_{i+1} + \mathbf{c}_{i+1}^\dagger \mathbf{c}_i \ . \tag{A.19}$$

Thus, in the fermionic representation, the XY Hamiltonian can be expressed as

$$\mathbf{H}_{XY} = -\frac{J}{2} \sum_{i=1}^{N} (\mathbf{c}_i^\dagger \mathbf{c}_{i+1} - \mathbf{c}_i \mathbf{c}_{i+1}^\dagger) \tag{A.20}$$

$$= -\frac{J}{2} \sum_{i=1}^{N} (\mathbf{c}_i^\dagger \mathbf{c}_{i+1} + \mathbf{c}_{i+1}^\dagger \mathbf{c}_i) \tag{A.21}$$

which can be exactly diagonalized.

A.3 Symmetry between S_z and H_{XY}

For the XY-model with a transverse magnetic field in the z-direction, the Hamiltonian, $\mathbf{H}_{XY}$, commutes with the z-spin operator, $\mathbf{S}^z$, creating a symmetry about the z-direction. In the following proof, both $\mathbf{S}^z$ and $\mathbf{H}_{XY}$ are expressed using operators.

$$[S^z, H_{XY}] = S^z(-J\sum_{i=1}^{N}(S_i^x S_{i+1}^x + S_i^y S_{i+1}^y)) - (-J\sum_{i=1}^{N}(S_i^x S_{i+1}^x + S_i^y S_{i+1}^y))S^z \tag{A.22}$$

$$= -J\sum_{i=1}^{N}(S^z S_i^x S_{i+1}^x + S^z S_i^y S_{i+1}^y - S_i^x S_{i+1}^x S^z - S_i^y S_{i+1}^y S^2) \tag{A.23}$$

$$= -J\sum_{i=1}^{N}([S^z, S_i^x S_{i+1}^x] + [S^z, S_i^y S_{i+1}^y]) \tag{A.24}$$

$$= -J\sum_{i=1}^{N}([S^z, S_i^x]S_{i+1}^x + S_i^x[S^z, S_{i+1}^x] + [S^z, S_i^y]S_{i+1}^y + S_i^y[S^z, S_{i+1}^y]) \tag{A.25}$$

$$== J\sum_{i=1}^{N}(iS_i^y S_{i+1}^x + iS_i^x S_{i+1}^y - iS_i^x S_{i+1}^y - iS_i^y S_{i+1}^x) \tag{A.26}$$

$$= 0\ . \tag{A.27}$$

Let's illustrate the symmetry with example eigenstates and eigenvalues of $\mathbf{S}_z$, $|M\rangle$ and λ_M and $|N\rangle$ and λ_N. For $|M\rangle \neq |N\rangle$,

$$\langle N|\,[S^z, H_{XY}]\,|M\rangle = \langle N|\,S^z H_{XY}\,|M\rangle - \langle N|\,H_{XY} S^z\,|M\rangle \tag{A.28}$$

$$= (\lambda_N - \lambda_M)\,\langle N|\,H_{XY}\,|M\rangle \tag{A.29}$$

$$= \langle N|\,H_{XY}\,|M\rangle = 0\ . \tag{A.30}$$

Since the eigenvalues λ_M and λ_N are different, the matrix elements of $\mathbf{H}_{XY}$ with different eigenstates of $\mathbf{S}^z$ must be zero. Thus, we show that the XY Hamiltonian can not couple with different values of $\mathbf{S}^z$ because of commuting operators.

A.4 Interaction Representation of the XY Model

A given time-dependent Hamiltonian $\mathbf{H}$ can be transformed into a unitary operator through continuous Trotterization.

$$\mathbf{U}(t,t_0) = T_t e^{-i\int_{t_0}^{t} dt' \mathbf{H}(t')} , \tag{A.31}$$

where T_t is the time ordering symbol. Substituting in the XY Hamiltonian in operator variables with magnetic fields in the x and z directions into Eq. (A.31),

$$\mathbf{U}(t,t_0) = T_t e^{-i\int_{t_0}^{t} dt' \{-J\sum_i (\sigma_i^x \sigma_{i+1}^x + \sigma_i^y \sigma_{i+1}^y) - B_x \sum_i \sigma_i^x - B_z(t')\sum_i \sigma_i^z\}} . \tag{A.32}$$

Using the Schrödinger equation, Eq. (A.32) satisfies

$$i\frac{d}{dt}\mathbf{U}(t,t_0) = \mathbf{H}(t)\mathbf{U}(t,t_0) . \tag{A.33}$$

To transform into the interaction representation, let

$$\begin{aligned}
\mathbf{H}_0(t) &= -B_z(t)\sum_i \sigma_i^z & \text{(A.34)}\\
\mathbf{V}(t) &= -\sum_i J(\sigma_i^x\sigma_{i+1}^x + \sigma_i^y\sigma_{i+1}^y) - B_x\sum_i \sigma_i^x & \text{(A.35)}\\
\mathbf{H}_{XY}(t) &= \mathbf{H}_0(t) + \mathbf{V}(t) & \text{(A.36)}\\
\mathbf{U}_0(t,t_0) &= e^{i\int_{t_0}^{t} B_z(t')\sum_i \sigma_i^z dt'} & \text{(A.37)}\\
\mathbf{U}(t,t_0) &= \mathbf{U}_0(t,t_0)\mathbf{U}_I(t,t_0) . & \text{(A.38)}
\end{aligned}$$

Let's define the Hamiltonian in the interaction representation as

$$i\frac{d}{dt}\mathbf{U}_I(t,t_0) = \mathbf{V}_I(t)\mathbf{U}_I(t,t_0) . \tag{A.39}$$

Substituting terms into Eq. (A.33),

$$\begin{aligned}
i\frac{d}{dt}\mathbf{U}(t,t_0) &= \mathbf{H}_0(t)\mathbf{U}(t,t_0) + \mathbf{U}_0(t,t_0)\mathbf{U}_0^\dagger(t,t_0)\mathbf{V}(t)\mathbf{U}_0(t,t_0)\mathbf{U}_I(t,t_0) & \text{(A.40)}\\
&= \mathbf{H}_0(t)\mathbf{U}(t,t_0) + \mathbf{U}_0(t,t_0)i\hbar\frac{d}{dt}\mathbf{U}_I(t,t_0) , & \text{(A.41)}
\end{aligned}$$

where

$$\mathbf{V}_I(t) = \mathbf{U}_0^\dagger(t,t_0)\mathbf{V}(t)\mathbf{U}_0(t,t_0) . \tag{A.42}$$

For simplicity, let's define $t_0 = 0$. The relationship in Eq. (A.39) gives

$$\mathbf{U}_I(t) = T_t e^{-i\int_0^t \mathbf{V}_I(t')dt'} . \tag{A.43}$$

Now solving for $\mathbf{V}_I(t)$,

$$\begin{aligned}\mathbf{V}_I(t) &= \mathbf{U}^\dagger(t)_0\mathbf{V}(t)\mathbf{U}_0(t) &(A.44)\\ &= e^{-i\int_0^t B_z(t')\sum_i\sigma_i^z}\{-\sum_i J(\sigma_i^x\sigma_{i+1}^x+\sigma_i^y\sigma_{i+1}^y)-B_x\sum_i\sigma_i^x\}e^{i\int_0^t B_z(t')\sum_i\sigma_i^z} &(A.45)\end{aligned}$$

Let

$$\theta(t)=\int_0^t B_z(t')dt' \ . \tag{A.46}$$

Substituting into Eq. (A.45),

$$\begin{aligned}\mathbf{V}_I(t) = &-\sum_i J(cos\theta(t)\sigma_i^x+sin\theta(t)\sigma_i^y)(cos\theta(t)\sigma_{i+1}^x+sin\theta(t)\sigma_{i+1}^y)\\ &-\sum_i J(-sin\theta(t)\sigma_i^x+cos\theta(t)\sigma_i^y)(-sin\theta(t)\sigma_{i+1}^x+cos\theta(t)\sigma_{i+1}^y)\\ &-\sum_i B_x(cos\theta(t)\sigma_i^x+sin\theta(t)\sigma_i^y)\end{aligned} \tag{A.47}$$

$$\mathbf{V}_I(t)=-J\sum_i(\sigma_i^x\sigma_{i+1}^x+\sigma_i^y\sigma_{i+1}^y)-B_x\sum_i(cos\theta(t)\sigma_i^x+sin\theta(t)\sigma_i^y) \ . \tag{A.48}$$

To find the total z-component of spin for a system, we can evaluate

$$\langle\psi|\,\mathbf{U}^\dagger(t)\sum_i\sigma_i^z\mathbf{U}(t)\,|\psi\rangle \tag{A.49}$$

$$=\langle\psi|\,T_t e^{i\int_0^t\mathbf{V}_I(t')dt'}e^{-i\int_0^t B_z(t')\sum_j\sigma_j^z}\sum_i\sigma_i^z e^{i\int_0^t B_z(t')\sum_j\sigma_j^z}T_t e^{-i\int_0^t\mathbf{V}_I(t')dt'}\,|\psi\rangle \ . \tag{A.50}$$

The $\mathbf{U}_0(t)$ term commutes with $\mathbf{S}_i^z$; therefore,

$$\begin{aligned}\langle\psi|\,\mathbf{U}^\dagger(t)\sum_i\sigma_i^z\mathbf{U}(t)\,|\psi\rangle &= \langle\psi|\,T_t e^{i\int_0^t\mathbf{V}_I(t')dt'}\sum_i\sigma_i^z T_t e^{-i\int_0^t\mathbf{V}_I(t')dt'}\,|\psi\rangle &(A.51)\\ &= \langle\psi|\,\mathbf{U}_I^\dagger(t)\sum_i\sigma_i^z\mathbf{U}_I(t)\,|\psi\rangle \ . &(A.52)\end{aligned}$$

Thus, we can also use the interaction representation of the XY Hamiltonian to find the total z-component of spin. We have removed the B_z dependence leaving only the B_x term in the new XY Hamiltonian given by Eq. (A.48). The time-dependent field is now given by Eq. (A.46).

Funding

This work was supported, in part, by the Department of Energy Office of Science, Basic Energy Sciences, under grant number DE-SC0019469.

Bibliography

[1] E. Ising, "Beitrag zur Theorie des Ferromagnetismus," *Zeitschrift für Physik*, vol. 31, no. 1, pp. 253–258, 1925. DOI: 10.1007/BF02980577.

[2] M. Born and V. Fock, "Beweis des Adiabatensatzes," *Zeitschrift für Physik*, vol. 51, no. 3, pp. 165–180, 1928. DOI: 10.1007/BF01343193.

[3] G. Pagano, A. Bapat, P. Becker, K. S. Collins, A. De, P. W. Hess, H. B. Kaplan, A. Kyprianidis, W. L. Tan, C. Baldwin, L. T. Brady, A. Deshpande, F. Liu, S. Jordan, A. V. Gorshkov, and C. Monroe, "Quantum approximate optimization of the long-range ising model with a trapped-ion quantum simulator," *Proceedings of the National Academy of Sciences*, vol. 117, no. 41, pp. 25 396–25 401, 2020. DOI: 10.1073/pnas.2006373117.

[4] C. Zener, "Non-adiabatic crossing of energy levels," *Proceedings of the Royal Society of London Series A*, vol. 137, pp. 696–702, 1932. DOI: 10.1098/rspa.1932.0165.

[5] P. Richerme, C. Senko, J. Smith, A. Lee, S. Korenblit, and C. Monroe, "Experimental performance of a quantum simulator: Optimizing adiabatic evolution and identifying many-body ground states," *Physical Review A*, vol. 88, no. 1, p. 012 334, 2013. DOI: 10.1103/PhysRevA.88.012334.

[6] A. Cervera-Lierta, "Exact ising model simulation on a quantum computer," *Quantum*, vol. 2, p. 114, 2018. DOI: 10.22331/q-2018-12-21-114. arXiv: 1807.07112.

[7] Z. Bian, F. Chudak, R. Israel, B. Lackey, W. G. Macready, and A. Roy, "Discrete optimization using quantum annealing on sparse ising models," *Frontiers in Physics*, vol. 2, p. 56, 2014. DOI: 10.3389/fphy.2014.00056.

[8] D. Zubov, F. Volponi, and M. Khosravy, "D-wave quantum computing ising model: A case study for the forecasting of heat waves," in *2015 International Conference on Control, Automation and Information Sciences (ICCAIS)*, 2015, pp. 149–152. DOI: 10.1109/ICCAIS.2015.7338651.

[9] G. Vidal and C. M. Dawson, "Universal quantum circuit for two-qubit transformations with three controlled-NOT gates," *Physical Review A*, vol. 69, no. 1, p. 010 301, 2004. DOI: 10.1103/PhysRevA.69.010301.

[10] B. Kraus and J. I. Cirac, "Optimal creation of entanglement using a two–qubit gate," *Physical Review A*, vol. 63, no. 6, p. 062 309, 2001. DOI: 10.1103/PhysRevA.63.062309. arXiv: quant-ph/0011050.

[11] M. A. Nielsen and I. L. Chuang, *Quantum computation and quantum information*, 10th anniversary ed. Cambridge ; New York: Cambridge University Press, 2010, 676 pp., ISBN: 978-1-107-00217-3.